THE JOURNAL OF PHYSICAL CHEMISTRY C

Article

pubs.acs.org/JPCC

Guest Hydrogen Bond Dynamics and Interactions in the Metal–Organic Framework MIL-53(Al) Measured with Ultrafast Infrared Spectroscopy

Jun Nishida and Michael D. Fayer*

Department of Chemistry, Stanford University, Stanford, California 94305, United States

Supporting Information

ABSTRACT: MIL-53(Al) is among the most "flexible" metal–organic frameworks and significantly changes its structure when guest molecules are introduced into the framework's pores. The guest molecules interact with μ_2-OH, which is a hydroxyl group bridging two aluminums. This interaction is thought to play an important role in the adsorption of molecules into the pores. Here, we report infrared absorption, infrared pump–probe, and two-dimensional infrared spectroscopy on a deuterated bridging hydroxyl, μ_2-OD, in MIL-53(Al) loaded with various guest molecules. Depending on guest, large vibrational frequency shifts, broadening of absorption band, enhancement of absorption coefficient, and acceleration of vibrational relaxation were observed, which are all signatures of hydrogen bonding interactions between the bridging hydroxyls and the guest. 2D IR spectroscopy reveals that the time evolution of the vibrational frequency occurs on multiple time scales: subpicosecond dynamics caused by localized hydrogen bond fluctuations and picosecond dynamics of the framework lattice, followed by significantly slower dynamics likely induced by global reconfigurations of the guest molecules in the pores. When benzonitrile, a strong hydrogen bonding agent, is introduced into the pores, an oscillatory feature was observed in the time evolution of the frequency, which was assigned to underdamped hydrogen bond fluctuations.

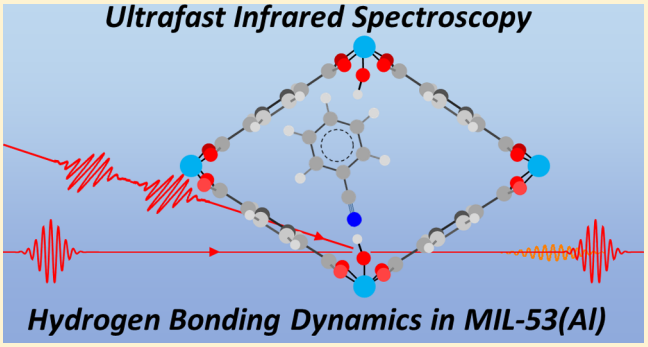

I. INTRODUCTION

In metal–organic frameworks (MOFs), metal atoms or inorganic metal clusters are connected by organic linkers to create regularly ordered nanopores. These nanopores can adsorb guest molecules, rendering the MOFs promising candidates for nanostructured gas storage systems[1] and selective filters for liquids.[2] The structures and properties of the MOFs depend on the types of metal clusters and organic linkers, which lead to a truly rich variety of MOFs and their applications. For example, zirconium-based UiO-66 MOF consists of three-dimensional octahedral and tetrahedral pores and shows high mechanical and chemical stability.[3] Therefore, UiO-66 MOF can support functional molecules as the catalysts for a variety of reactions.[4]

In contrast, some MOFs show an intriguing property that their pores undergo structural changes upon the introduction of guest molecules.[5−7] These MOFs are often referred to as flexible MOFs, and their flexibility is considered as a key factor for enhanced capacity and selectivity in gas adsorption process. MIL-53(Al) is a representative flexible MOF.[8] In MIL-53(Al), aluminum atoms are joined by benzene-1,4-dicarboxylate (BDC) linkers and bridging hydroxyls (μ_2-OH) to form one-dimensional channels (Figure 1A,B). It has been shown by powder X-ray studies that the pores are substantially deformed when they are loaded with guest molecules.[8] This guest-induced deformation of the structure is often referred to as "breathing" motion of the MOF. There have been indications that hydrogen bonding between guest molecules and the μ_2-OH in the framework leads to the deformaton.[5,9] Thus, it is useful to characterize both the time-averaged and dynamical nature of hydrogen bond interactions between the framework and guest molecules.

Infrared spectroscopy has been very successful in studying hydrogen bonding interactions in many systems. When a hydroxyl forms a hydrogen bond with an acceptor, several distinct changes are known to be induced in the hydroxyl stretch infrared absorption band; there is a red-shift in the resonance frequency, an enhancement of the absorption cross section, and often broadening of the absorption band. These features in infrared absorption spectra are often so clear that they are important criteria associated with hydrogen bonding.[10] In addition, advances in ultrafast infrared spectroscopy have made it possible to monitor the fluctuations of the hydrogen bond on subpicosecond to 100 ps time scales. Ultrafast infrared spectroscopy has provided insights into the dynamics of various

Received: March 15, 2017
Revised: April 27, 2017
Published: April 28, 2017

DOI: 10.1021/acs.jpcc.7b02458
J. Phys. Chem. C 2017, 121, 11880−11890

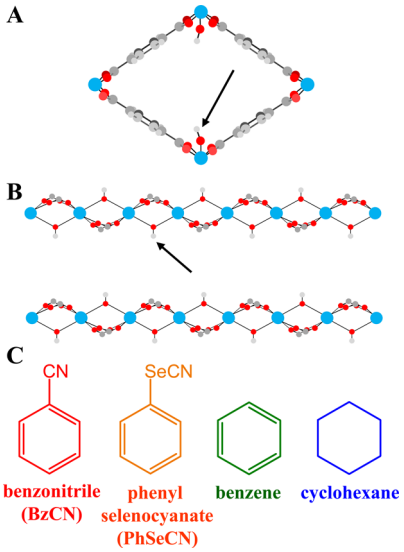

Figure 1. (A, B) Schematic illustrations of MIL-53(Al) MOF structure from the front view (A) and the side view (B). Aluminum atoms (blue) are connected by benzene-1,4-dicarboxylate (BDC) linkers and bridging hydroxyls (μ_2-OH). Note that in the side view (B) only the terminal carboxylate groups of the BDC linkers are shown for clarity. The μ_2-hydroxyls (arrows) are facing into the one-dimensional pore channels and are expected to form hydrogen bonds with guest molecules. (C) The four guest molecules introduced into the MIL-53(Al) pores.

molecular systems, from bulk water to proteins, supercooled liquids, and ionic liquids.[11−22]

The investigation of MOFs with ultrafast infrared spectroscopy has become possible due to the significant improvements in both experimental and theoretical methodologies.[23−26] Here we report the application of infrared vibrational spectroscopy to elucidate both the time-averaged and the dynamical nature of the interactions between various guest molecules and the bridging hydroxyls in MIL-53(Al) frameworks. The bridging hydroxyls were partly deuterated to yield μ_2-OD, and the stretching vibration of this key hydroxyl was studied using several methods. Infrared absorption spectroscopy clearly revealed that μ_2-OD forms hydrogen bonds with guest molecules, and the strength of the hydrogen bonds depends on guest molecule as seen by the shifts in the peak position. Infrared pump−probe spectroscopy showed that stronger hydrogen bonds lead to faster population relaxation of the excited OD vibration. The nature of the framework−guest interactions, however, was most clearly seen in the dynamics of the hydrogen bonds probed by two-dimensional infrared (2D IR) spectroscopy. 2D IR spectroscopy monitors the temporal fluctuations of the hydrogen bonding strength occurring on subpicosecond to subnanosecond time scales. The results show that the hydrogen bond evolves on three distinct time scales (subps, ~ps, and >subns), corresponding to the local hydrogen bonding dynamics, framework lattice motion, and the reconfiguration of guest molecules, respectively. When benzonitrile, a strong hydrogen bonding acceptor, forms a hydrogen bond with μ_2-OD, we observed an underdamped oscillatory feature in the temporal evolution of the hydrogen bonding strength. Possible origins of this oscillatory feature are discussed.

2D IR spectroscopy was previously applied to another metal−organic framework, UiO-66, functionalized with an iron−carbonyl complex as a vibrational probe.[23] Here, the bridging hydroxyls, which are native to the framework, are used as the vibrational probe. The dynamics inside the MOF were probed directly without the chemical modification associated with introducing a bulky vibrational probe. The bridging hydroxyl participates in the hydrogen bond formation between the framework and the guest molecules, enabling direct characterization of the hydrogen bonding.

II. RESULTS AND DISCUSSION

A. Sample Preparation and Characterization. Commercially obtained MIL-53(Al) particles (Basolite A100, Sigma-Aldrich) were activated,[8] deuterated,[27] and loaded with various solvents: benzonitrile (BzCN), phenyl selenocyanate (PhSeCN), benzene, and cyclohexane (see Figure 1C). The detailed sample preparation procedures are given in the Supporting Information. The deuterated μ_2-hydroxyl, μ_2-OD, shows a resonant absorption between 2635 and 2735 cm^{-1} depending on the guest molecules. This frequency range is covered by the tunable frequency range of the infrared pulses. The experiments are conducted with an infrared pulse shaping system using a germanium acousto-optic modulator (AOM),[28,29] which is necessary for pump−probe and 2D IR spectroscopy discussed later. BzCN and PhSeCN were readily adsorbed into the pores. The frameworks loaded with BzCN and PhSeCN were prepared by immersing the activated MIL-53(Al) in BzCN or PhSeCN overnight. The external liquid was removed from the MOFs using suction filtration under a constant flow of very dry air. The thermogravimetric analysis (TGA) showed that the frameworks loaded with BzCN in this manner contained 0.93 BzCN per one μ_2-hydroxyl (Figure S1A). The framework loaded with PhSeCN might contain bulk PhSeCN which was not fully removed by the filtration process (Figure S1B), but such PhSeCN does not affect our measurement on μ_2-OD located inside the pore. For the infrared spectroscopy experiments, the particles were immersed in paraffin oil for index matching. Because benzene and cyclohexane tended to come out of the pores, the activated MIL-53(Al) was immersed in benzene or cyclohexane in the sample cell for the infrared experiments so that the pores are filled with the guest molecules, and the sample is isolated from atmospheric water. When measurements on the MIL-53(Al) with empty pores were performed, the activated particles were sealed in the sample cell in a glovebox to prevent absorption of atmospheric water.

B. Infrared Absorption Spectroscopy. FT-IR spectra of μ_2-OD stretch in MIL-53(Al) loaded with the four different guest molecules and with empty pores are shown in Figure 2A. Each absorption band was normalized at the peak maximum. The background subtraction procedure is outlined in the Supporting Information (Figure S2). When the pore is empty (no guest molecule), μ_2-OD shows a resonant absorption at a very high frequency of 2733 cm^{-1}. For comparison, deuterated methanol (CH_3OD) in the gas phase has its OD stretch absorption at 2720 cm^{-1}.[30] Thus, μ_2-OD in empty pores appears to be well isolated from interactions with other moieties.

With guest molecules in the pores, the μ_2-OD resonant frequency shifts to the red. The amount of the shift strongly depends on the guest molecules, and when BzCN, a strong hydrogen bond acceptor, is introduced, a very large red-shift of ~90 cm^{-1} was observed, indicating that a well-defined hydrogen bond is formed between a guest BzCN and a

DOI: 10.1021/acs.jpcc.7b02458
J. Phys. Chem. C 2017, 121, 11880−11890

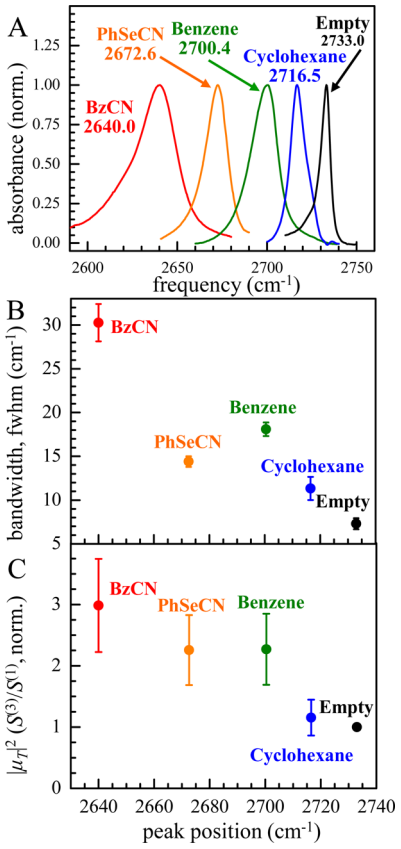

Figure 2. (A) Infrared absorption spectra of μ_2-OD in the MIL-53(Al) framework with various guest molecules. A large shift from the peak position with an empty pore (2733.0 cm^{-1}) indicates a formation of a well-defined hydrogen bond. (B) Absorption line widths (fwhm) from the absorption spectra in (A). The line widths are reasonably well correlated with the peak positions, i.e., hydrogen bond strength. (C) Normalized squared transition dipole moments estimated by comparing linear absorption signals and pump−probe signals. The transition dipole moment is enhanced as a stronger hydrogen bond acceptor is introduced into the pore.

framework μ_2-OD. Different guest molecules form hydrogen bonds with various strength. It is clear from Figure 2A that PhSeCN forms a weaker hydrogen bond with μ_2-OD than BzCN, as it shows an ~60 cm^{-1} red-shift as opposed to an ~90 cm^{-1} shift with BzCN. It is reasonable to assume that μ_2-OD is interacting with the nitrile (CN) group of BzCN and PhSeCN; in BzCN, the CN group is directly conjugated with the aromatic ring, and the nitrogen atom is therefore supplied with additional electron density, while in PhSeCN, the selenium atom blocks the direct conjugation between aromatic ring and CN. Therefore, BzCN is expected to be a stronger hydrogen bond acceptor than PhSeCN, which is consistent with the spectral shifts.

Remarkably, when benzene is the guest, μ_2-OD shows an ~33 cm^{-1} red-shift, which is significantly larger than the ~17 cm^{-1} shift with cyclohexane in the pores. The molecular shapes, sizes, and the dielectric constants for benzene (ε = 2.27) and cyclohexane (ε = 2.02) are fairly close. Thus, this significant difference in the peak shifts is unlikely to be caused by a difference in the solvent reaction fields formed by benzene and cyclohexane. It has previously been shown that benzene forms a well-defined complex with phenol through OH···π hydrogen bonding.[31,32] It is likely that similar π hydrogen bonding is formed between benzene and μ_2-OD in the framework. In contrast, because cyclohexane is unlikely to form a well-defined hydrogen bond with a hydroxyl, the ~17 cm^{-1} shift caused by the introduction of cyclohexane into the pores is induced by a nonspecific interaction, such as a dipole−induced dipole interaction.[33]

As seen in Figure 2A, in addition to the peak positions, the absorption line widths vary. The line width (full width at half-maximum, fwhm) with respect to the peak position is plotted in Figure 2B. It can be seen that the line width is well correlated with the peak position as an indicator of the hydrogen bonding strength; a stronger hydrogen bond tends to yield a broader absorption band. The broadening of the absorption band can be caused by two mechanisms, namely homogeneous broadening and inhomogeneous broadening.[34] To fully characterize the variance of the bandwidth, these two contributions must be separated. This separation will be achieved using two-dimensional infrared spectroscopy as discussed in section E. With strong hydrogen bond acceptors introduced, the observed absorption line shapes are somewhat asymmetric, with broadening observed on the red sides of the bands. These asymmetries can arise from possible distinct configurations of the guest molecules in the pores or from the non-Condon effect in which the absorption cross section varies across the band. The non-Condon effect is known to occur in hydrogen bonding systems with the cross section increasing on the red side of the line.[22,35]

Another important criterion for the hydrogen bond formation is the enhancement of the absorption cross section. The absorption cross section is proportional to the square of the transition dipole moment magnitude, $|\mu_T|^2$. As discussed in the Supporting Information, $|\mu_T|^2$ was evaluated by comparing the absorbance ($S^{(1)} \propto |\mu_T|^2$) and the pump−probe signal amplitude ($S^{(3)} \propto |\mu_T|^4$). Figure 2C shows the plot of $S^{(3)}/S^{(1)} \propto |\mu_T|^2$ for different guest molecules with respect to the peak positions. $|\mu_T|^2$ for the empty pore was normalized to 1, and the other $|\mu_T|^2$ s were scaled to the empty pore values. It is evident that the peak position and the cross section are correlated. The cross section is significantly enhanced by a hydrogen bond acceptor in the pore. While the enhancement is obvious when BzCN, PhSeCN, and benzene are introduced, the enhancement by cyclohexane is relatively minor, supporting the idea that cyclohexane is not forming a well-defined hydrogen bond with the bridging hydroxyl.

C. Infrared Pump−Probe Spectroscopy. Polarization-selective pump−probe (PSPP) spectroscopy was applied to the bridging hydroxyl, μ_2-OD. Experimental details of the PSPP experiment can be found in the Supporting Information. The PSPP experiment is essentially transient absorption spectroscopy where pump and probe pulses have an identical infrared spectral profile. The spectra of the infrared pulses were centered at the peak positions of μ_2-OD (Figure 2A) for each sample, with the spectral bandwidth of >90 cm^{-1} fwhm. In the PSPP experiment, μ_2-OD is pumped first by a polarized "pump" pulse, which brings some of the vibrational ground state population to the first vibrational excited state. After some waiting time, t, the second "probe" pulse crosses in the sample. The polarization of the probe pulse is either parallel or perpendicular to the pump pulse. Because the pump pulse has bleached the ground state population, the absorption in the probe pulse by μ_2-OD is reduced. The resultant increase in the probe transmission is the pump−probe signal. The signal amplitude depends on the time t between the pump and probe

DOI: 10.1021/acs.jpcc.7b02458
J. Phys. Chem. C 2017, 121, 11880−11890

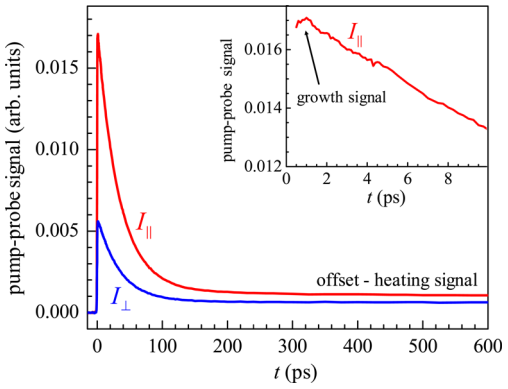

Figure 3. Dependence of the pump−probe signal on the delay time t for μ_2-OD bound to BzCN. $I_{\parallel}(t)$ and $I_{\perp}(t)$ were acquired by setting the polarizations of the two pulses parallel and perpendicular, respectively. The unwanted artifacts, a heating signal and a growth signal, were removed as described in the Supporting Information before the data were further processed to yield the population decays and the anisotropy decays.

pulses. The pump−probe signals for the parallel and perpendicular polarizations are denoted as $I_{\parallel}(t)$ and $I_{\perp}(t)$, respectively. Figure 3 shows data for μ_2-OD bound to BzCN.

The pump−probe signals, as shown in Figure 3, contained two types of features other than those that provide the desired information. First, well-known "heating" signals were observed as offsets in the data (signal above zero with no slope) at very long times in the pump−probe signals.[11] Also, at early time (<2 ps) a growth in the signal amplitude was observed (Figure 3, inset). The same growth signal was observed in nondeuterated MIL-53(Al) powders which do not have resonant vibrational modes in the 2640−2730 cm^{-1} region. Therefore, the growth signal is definitely not μ_2-OD in origin and may arise from minor contaminants in the sample, such as Al_2O_3. These extra signals were removed quantitatively; the detailed procedure is found in the Supporting Information (Figure S3).

Using the measured $I_{\parallel}(t)$ and $I_{\perp}(t)$, the normalized population decay, $P(t)$, and the anisotropy decay, $r(t)$, can be constructed as[36]

$$P(t) = (I_{\parallel}(t) + 2I_{\perp}(t))/3 \quad (1)$$

$$r(t) = \frac{I_{\parallel}(t) - I_{\perp}(t)}{I_{\parallel}(t) + 2I_{\perp}(t)} \quad (2)$$

The population decay, $P(t)$ (see Figure 4 for all samples), is proportional to the number of μ_2-OD in the vibrationally excited state. The anisotropy, $r(t)$ (see Figure 5 for BzCN-loaded sample), gives the orientational relaxation correlation function (second Legendre polynomial correlation function). Because the angular motion of the μ_2-ODs is highly restricted in the MOF, the orientation of μ_2-OD does not randomize and $r(t)$ does not decay to zero. However, μ_2-OD can sample a small range of angles, and such restricted orientational motion can be described well by the "wobbling-in-a-cone" model[37,38] as discussed below.

Figure 4A shows the population decays, $P(t)$, obtained from PSPP experiments for μ_2-OD bound to various guest molecules and with the pores empty. Each decay was fit with single exponential ($\propto \exp[-t/\tau_V]$), and the vibrational relaxation rate $k_V \equiv 1/\tau_V$ was plotted with respect to the peak positions obtained from the FT-IR measurements (Figure 4B).

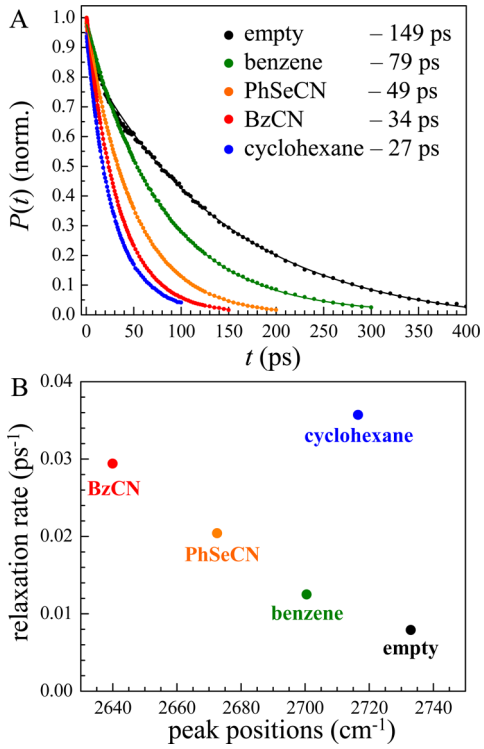

Figure 4. (A) Population decays extracted from the pump−probe signals and eq 1. The decays were fitted with single exponentials giving the vibrational relaxation times, τ_V. (B) Vibrational relaxation rates calculated as $k_V \equiv 1/\tau_V$, which correlate well with the peak positions in the infrared absorption spectra (Figure 2A).

When the pore is empty, μ_2-OD has a long vibrational lifetime of 149 ps. Considering OD vibrations in bulk liquids typically have lifetimes of 2−20 ps,[22,39,40] this lifetime is remarkably long. As hydrogen bond acceptors are introduced into the pores, the vibrational lifetime is reduced. Particularly for BzCN, the lifetime is 34 ps, which is roughly factor of 5 acceleration of the vibrational relaxation. As seen in Figure 4B, the vibrational relaxation rates are remarkably well correlated with the absorption peak positions as indicators for hydrogen bonding strength, except for the guest molecule cyclohexane.

The trend in the vibrational relaxation rate can be understood by considering the mechanism of the vibrational relaxation. For the vibrational relaxation to take place, the vibrational energy of the μ_2-OD stretching mode must relax into the other modes of the system, so that the total energy is conserved.[41] The relaxation rate is mainly determined by how many modes of the system are required to conserve energy and how strongly each of the accepting modes is coupled to the μ_2-OD stretching mode.

When the pore is empty, the only possible direct relaxation pathway is to the μ_2-OD bend and the O−Al vibrational modes. If a combination of these modes does not match the μ_2-OD stretch frequency, then conservation of energy will require phonons of the MOF framework, which are indirectly coupled to μ_2-OD stretch mode. Because of the limited number of accessible system modes and their weak coupling to the μ_2-OD stretch mode, the vibrational lifetime is very long, 149 ps.

It is clear from the measurements that the introduction of the guest molecules provides additional pathways for the vibrational energy to be dissipated, shortening the μ_2-OD lifetime. The guest molecules provide more modes into which the μ_2-

DOI: 10.1021/acs.jpcc.7b02458
J. Phys. Chem. C 2017, 121, 11880−11890

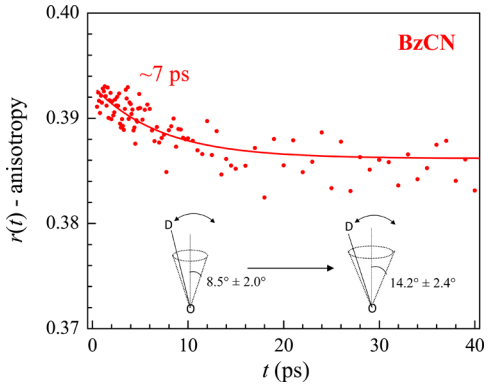

Figure 5. Anisotropy decay for μ_2-OD bound to BzCN obtained from the pump−probe signals and eq 2. The decay was fitted with a single exponential with a large offset, indicating that the O−D bond undergoes inertial reorientation rapidly over an ~8.8° cone angle and then diffuses with a time constant of ~7 ps over an ~12.4° cone angle.

OD stretch mode energy can be dissipated. The stronger hydrogen bond enhances the coupling between the μ_2-OD stretch mode and the guest molecules' modes, leading to the faster vibrational relaxation rates as observed in Figure 4B.

The exceptionally fast vibrational relaxation with cyclohexane as the guest is not explained by a very strong hydrogen bond. Cyclohexane does not hydrogen bond to the μ_2-OD. However, cyclohexane has more vibrational modes around the vibrational energy of μ_2-OD (2716.5 cm^{-1}) than the other guest molecules (Figure S2). In addition, the cyclohexane ring is not as stiff as the benzene moiety and therefore has more low-frequency modes. Furthermore, cyclohexane is likely to solvate the μ_2-OD hydroxyls with nondirectional interactions, which may make more vibrational modes of cyclohexane directly accessible for vibrational relaxation. Thus, the anomalously fast relaxation rate may indicate that cyclohexane is interacting with the hydroxyls in a fundamentally different manner from the other guest molecules.

Figure 5 shows the anisotropy decay, $r(t)$, for μ_2-OD bound to BzCN. The anisotropy $r(t)$ is related to the wobbling motion of μ_2-OD by[36]

$$r(t) = 0.4\left\langle \frac{3(\hat{\mu}(0)\cdot\hat{\mu}(t))^2 - 1}{2} \right\rangle \quad (3)$$

where $\hat{\mu}(0)$ and $\hat{\mu}(t)$ are unit vectors parallel to a particular O−D bond at time 0 and t, and $\langle ... \rangle$ is the ensemble average over all the μ_2-ODs in a sample. If μ_2-OD does not move at all during the waiting time t and thus $\hat{\mu}(0)\cdot\hat{\mu}(t) = 1$, the anisotropy $r(t)$ yields the maximum possible value of 0.4. Based on the single-exponential fit to the data, even at $t = 0$, the anisotropy value yields 0.393 ± 0.003, smaller than 0.4. This small deviation from 0.4 indicates that μ_2-OD undergoes ultrafast highly restricted inertial motion with 8.5 ± 2.0° half-cone angle based on the "wobbling-in-a-cone" model (see Figure 5).[37,38,42] Then, the anisotropy decays with ~7 ps time constant by a small amount to an offset level of 0.381 ± 0.006. This decay shows that the μ_2-OD undergoes a small degree of diffusive angular relaxation (wobbling) with an angular diffusion constant of ~0.01 ps^{-1}. The diffusive wobbling samples a wider range of angles, a 14.2 ± 2.4° half-cone angle.[43]

The anisotropy decay demonstrates that μ_2-OD undergoes highly restricted angular motion. The limited angular motion is expected as the bridging hydroxyl is locked into position as a part of the framework. Although small, the angular motion provides some insight into the framework flexibility. Anisotropy decays for μ_2-OD interacting with the other guest molecules were also measured, and within the error, we were not able to discern any trends in the wobbling motion with respect to the hydrogen bonding strength. The details are discussed in the Supporting Information (Figure S4). The wobbling motion of μ_2-OD is not very sensitive to the nature of its interaction with guest molecules and therefore is a property of the framework itself.

D. Two-Dimensional Infrared (2D IR) Spectroscopy: CLS Analysis. To characterize the time evolution of the framework−guest interaction, we applied 2D IR spectroscopy to μ_2-OD in MIL-53(Al). As seen and discussed in Figure 2A, the infrared absorption bands have finite and varying bandwidths depending on the guest molecules. The broadening of the absorption band, particularly for the guests that form hydrogen bonds with μ_2-OD, likely arises from the variations in the hydrogen bond strength. For example, the μ_2-ODs interacting with BzCN has an ~30 cm^{-1} fwhm bandwidth. The hydroxyls giving rise to the red side of the band are forming stronger hydrogen bonds than the hydroxyls contributing to the blue side of the band.[13] The hydrogen bond strengths evolve with time due to the dynamics occurring in the framework, such as fluctuations of the hydrogen bond length, framework lattice structure fluctuations, and changes in the configuration of guest molecules in the pores. As a result, hydroxyls initially having a particular frequency within the inhomogeneously broadened absorption band will undergo spectral diffusion, i.e., sampling of frequencies that are different from their initial frequency. At sufficiently long time, the hydroxyls will sample all frequencies in the line. Thus, the frequency evolution is caused by structural fluctuations, and by monitoring the time evolution of the vibrational frequencies, the time dependence of the structural evolution is determined.

2D IR spectroscopy monitors the temporal evolution of the vibrational frequencies in subpicosecond to hundreds of picoseconds time scale. In 2D IR spectroscopy, the pump pulse in pump−probe experiment is split into two pulses separated by time τ (see Figure 6A).[28] This set of two pump pulses essentially labels the initial frequencies (ω_τ, horizontal axis of the 2D spectrum) of the hydroxyl stretches, and after waiting time T_w, the final frequencies (ω_m, vertical axis of the 2D spectrum) are read out by the third probe pulse and recorded by the emitted vibrational echo signal pulse. Note that the waiting time T_w is equivalent of t in pump−probe spectroscopy. Experimentally, the initial frequency ω_τ labeled by the first two pump pulses can be acquired by scanning τ, and the final frequency ω_m is obtained as the optical frequencies of the echo pulse. A more rigorous and complete description of 2D IR spectroscopy is provided in previous publications,[28,29,44] and the detailed implementation is described in the Supporting Information. The application of 2D IR spectroscopy to samples like MOFs, which are composed of macroscopic particles, is difficult because scattered light from the sample can significantly distort or overwhelm the 2D spectrum. This problem was recently overcome by combining AOM pulse shaping with an eight shot phase cycling/chopping sequence and polarization filtering to yield 2D spectra free from scatter artifacts.[23,27,45]

Figure 6B shows 2D IR spectra of μ_2-OD in MIL-53(Al) loaded with BzCN at T_w = 0.5 ps and T_w = 50 ps. A 2D IR spectrum is essentially a correlation plot between the initial

DOI: 10.1021/acs.jpcc.7b02458
J. Phys. Chem. C 2017, 121, 11880−11890

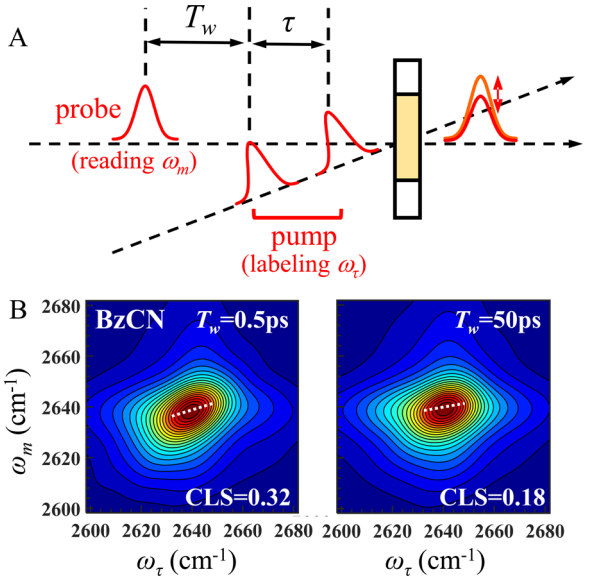

Figure 6. (A) Schematic illustration of two-dimensional infrared (2D IR) spectroscopy. The pump pulse in the pump−probe spectroscopy is further split into two pulses, and the set of the two pump pulses label the initial frequencies, ω_τ. After waiting time T_w, the probe pulse reads out the final frequencies, ω_m. (B) 2D IR spectra for μ_2-OD bound to BzCN at the waiting time T_w of 0.5 ps (left) and 50 ps (right). Center line slopes (CLS) are plotted in the 2D spectra as dashed white lines. The significant change in the CLS values indicates that structural dynamics occurred during the 50 ps time span.

(ω_τ) and the final (ω_m) frequencies separated by the waiting time T_w. When the waiting time T_w is small, ω_τ and ω_m tend to be about the same, that is, well correlated; as a result, the 2D band shape will be diagonally elongated. As T_w becomes longer, the dynamics occurring in the framework randomize the vibrational frequencies (spectral diffusion). Consequently, ω_τ and ω_m will lose correlation, yielding a more rounded band shape. Thus, by monitoring the evolution of the 2D band shape, the spectral diffusion dynamics can be extracted. The 2D band shape can be quantitatively evaluated by center line slope (CLS) method (Figure 6B, white dotted lines).[46,47] When ω_τ and ω_m are completely correlated, the CLS yields the maximum value of 1. As the two frequencies become uncorrelated by structural fluctuations, the CLS decays to 0. More quantitatively, a CLS is proportional to a frequency−frequency correlation function (FFCF) defined as $\langle \delta\omega(0)\delta\omega(T_w)\rangle$, where $\delta\omega(0) \equiv \omega(0) - \langle\omega\rangle$ and $\delta\omega(T_w) \equiv \omega(T_w) - \langle\omega\rangle$ and are deviations of a vibrational frequency from an average frequency at time 0 and T_w for a particular molecule, and $\langle ... \rangle$ means the ensemble average. The details are discussed in section E. Note that as shown in Figure 6B, CLSs were extracted around the centers of the two-dimensional peaks to avoid influence from the slight asymmetry observed on the red sides of the absorption line shapes.

2D IR spectra of μ_2-OD in MIL-53(Al) loaded with various guest molecules were acquired with varying T_ws, and the CLS was obtained for each set of spectra. The small heating contribution to the 2D spectrum, which grows in with the vibrational relaxation lifetime, was removed using the standard procedure.[11] See Supporting Information for details.

The CLS decays of μ_2-OD in MIL-53(Al) obtained with different guest molecules in the pores and empty pore are plotted in Figure 7. All of the CLS decays have a common feature, i.e. a very fast decay occurring in ≤∼2 ps followed by slow dynamics occurring over ≥∼100 ps. To quantify the dynamics with the two time scales, we fit the CLS data with a single-exponential decay after 8 ps. The CLS fit for ≥8 ps was extrapolated to earlier time and subtracted from the observed CLS decay to obtain the very fast decay component. The short time CLS decays are plotted in Figure 8. While it is difficult to find a trend in the slower dynamics in Figure 7, the fast dynamics displayed in Figure 8 show the behavior that is correlated with the hydrogen bonding strength; it is evident in Figure 8 that μ_2-OD bound to a hydrogen bonding acceptor exhibits faster dynamics.

Even when the pore is empty, the early CLS decays with 1.3 ps time constant (Figure 8E). Because the μ_2-OD does not interact with a guest molecule when the pore is empty, the 1.3 ± 0.1 ps spectral diffusion must be caused by structural fluctuations of the flexible framework; when the framework's structure fluctuates, the different framework configurations change the resonant frequency of the μ_2-OD, giving rise to the spectral diffusion.[23] When cyclohexane is introduced into the pores, we observed essentially the identical 1.4 ± 0.1 ps dynamics (Figure 8D), indicating that the spectral diffusion of the μ_2-OD is caused by framework structural fluctuations as observed for the empty pores. Apparently, the dynamics of cyclohexane itself are not inducing spectral diffusion, suggesting that the dynamics of the cyclohexane are highly restricted on very short time scales.

A clear change starts occurring to the early CLS decays when the hydrogen bonding acceptors are introduced into the pores. The early CLS decay for μ_2-OD bound to benzene is no longer single exponential, and it is fit well with biexponential with the time constants of 0.24 ± 0.08 and 1.8 ± 0.3 ps (Figure 8C). The latter time constant may arise from the framework fluctuations because the time constant is reasonably close to that of the empty pore, though the amplitude of the decay is much lower. On top of the framework fluctuations, a much faster dynamics, 0.24 ± 0.08 ps, is causing spectral diffusion with a significant amplitude. When much stronger hydrogen bonding acceptors, BzCN and PhSeCN, are added, ∼1 ps time constants are no longer observed, and the early CLS decays are dominated by subpicosecond dynamics, 0.34 ± 0.05 ps for BzCN and 0.45 ± 0.07 ps for PhSeCN, respectively (Figure 8A,B). Note that the short time CLS decay for the μ_2-OD bound to BzCN displays an oscillation, which is discussed in depth in section F.

The appearance of the subpicosecond components in the CLS decays can be understood as the signatures of the presence of hydrogen bonds. There are important insights into the origin of subpicosecond spectral diffusion components from previous studies of several hydrogen bonding systems. When the spectral diffusion of the O−D stretch of HOD molecules in H_2O were studied, ∼0.4 ps dynamics were observed. MD simulations demonstrated that this very fast component originates mainly from hydrogen bond length fluctuations with some contribution from angular fluctuations.[11] Similar ∼0.4 ps spectral diffusion dynamics were observed for O−D stretch modes for HOD, CD_3OD, and C_2D_5OD dissolved in the ionic liquid $EmimNTf_2$ where the O−D groups form hydrogen bonds with anions in the ionic liquid.[22] It is thus reasonable to assign the observed early CLS decay time constants of the μ_2-OD (0.34 ps with BzCN, 0.45 ps with PhSeCN, and 0.24 ps with benzene (Figure 8A−C)) to local hydrogen bond length fluctuations as well. While there is experimental error for these three values,

DOI: 10.1021/acs.jpcc.7b02458
J. Phys. Chem. C 2017, 121, 11880−11890

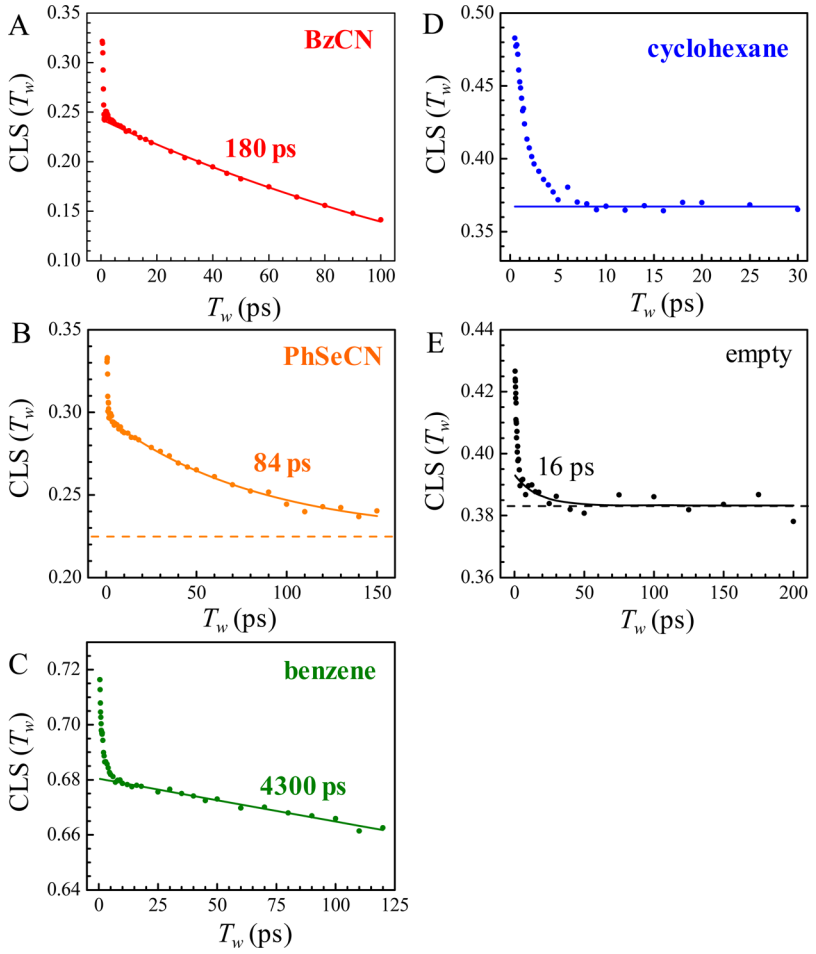

Figure 7. Dots: the CLS decays extracted from the measured 2D IR spectra for μ_2-OD bound to various guest molecules. Note that the T_w axes are different due to the different vibrational lifetimes, which limit the observable T_w window. All of the decays have a common feature; very fast decays occurring in <5 ps are followed by relatively slow dynamics. Solid lines: fits for the observed CLSs after T_w = 8 ps. The time constants are the single-exponential decay times. For BzCN and benzene, the CLSs were fitted without offsets. For PhSeCN and the empty pore, the CLSs were fitted with single exponential with an offset; the offset levels are indicated by the dotted lines. For cyclohexane, the CLS did not decay after T_w = 8 ps and was fitted with a constant.

the small variations may arise from the complex interplay among the hydrogen bonding strength, the mass of the molecules, and the extent of the confinement of each of the guest molecules.

While the early CLS decays of the μ_2-ODs with the guests BzCN and PhSeCN are completely dominated by the local hydrogen bond fluctuations (Figure 8A,B), the μ_2-OD with benzene shows spectral diffusion arising from both the local hydrogen bond fluctuations and framework fluctuations (Figure 8C). The results suggest that BzCN and PhSeCN form strong enough hydrogen bonds with the μ_2-OD that the hydrogen bond strength completely determines the inhomogeneity of the μ_2-OD vibrational frequency. In contrast, benzene forms a relatively weak π-hydrogen bond, so that both the local hydrogen bond strength variations and the framework structural fluctuations affect the μ_2-OD vibrational frequency.

As seen in Figure 7, the early CLS decays discussed above do not complete the spectral diffusion; the CLS is well above zero even at long time. The early CLS are all followed by much slower dynamics, the time constants of which strongly depend on the guest molecules. When the pore is empty, the CLS appears to be constant after ~10 ps (Figure 7E). Again, when the pore is empty, the framework structural variations are the only factor that can alter the resonant frequency of μ_2-OD, and therefore the incomplete spectral diffusion by 200 ps indicates the existence of much slower framework dynamics. It has been suggested by NMR measurements that π-flipping of the BDC linkers in the framework occurs on a time scale slower than ~1 μs.[48] Another possibility is the existence of static inhomogeneity caused by framework defects such as missing linkers. When the pores are filled with guest molecules, the global reconfiguration of the guest molecules in the pore, such as reorientation and translation, will certainly affect the vibration frequency of μ_2-OD and induce the slower spectral diffusion observed in Figure 7A–C. While the exact time constants for these slower dynamics are again determined by various factors such as the size of the molecules, the hydrogen bond strength, the mass of the molecules, and the framework structure surrounding the guest molecules, it is clear that the spectral diffusion is occurring on a much slower time scale than the dynamics in bulk liquid, indicating that the guest molecule dynamics are strongly influenced by confinement in the pores.

E. Absorption Band Broadening Mechanism. Figures 2A and 2B show that the absorption bandwidth is correlated with the hydrogen bond strength formed between the guest molecules and the μ_2-OD. However, the exact broadening

DOI: 10.1021/acs.jpcc.7b02458
J. Phys. Chem. C 2017, 121, 11880–11890

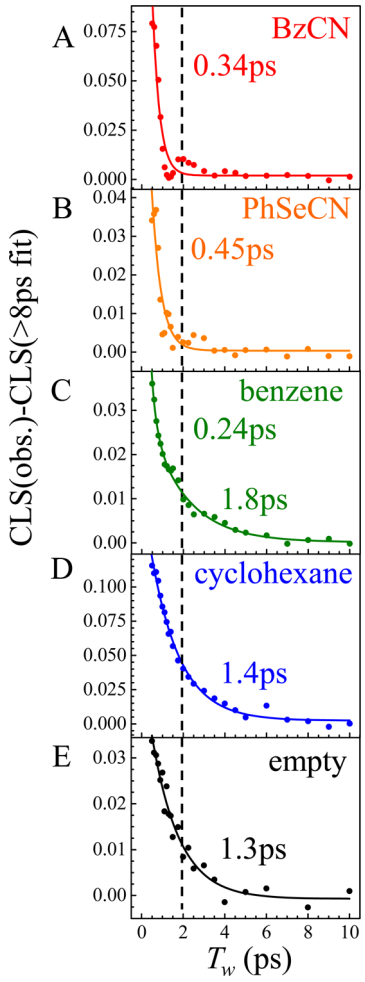

Figure 8. Fits to the CLS after T_w = 8 ps were extrapolated to earlier waiting times and subtracted from the observed CLSs to extract the early time components of the CLS decays. It is evident that μ_2-OD exhibits faster spectral diffusions at early times when a hydrogen bonding molecule is introduced into the pores.

mechanism of the band is not clear from the absorption spectra. Based on the CLS decays acquired from the 2D IR spectra, the broadening mechanism can be addressed.

Each absorption band line shape in Figure 2A is determined by a frequency−frequency correlation function (FFCF) of μ_2-OD bound to a guest molecule, which was modeled with a simplified Kubo form given by[34]

$$\langle \delta\omega(0)\delta\omega(t)\rangle = \sum_i \Delta_i^2 e^{-t/\tau_i} \quad (4)$$

τ_i is the time constant for ith process, and Δ_i is the frequency range sampled by that process. Each term in the summation contributes to the observed 1D absorption line shape. The manner each term contributes to the 1D line shape depends on the relationship between the fluctuation amplitude Δ_i and the dynamical time constant τ_i. If $\Delta_i \times \tau_i \ll 1$, motional narrowing occurs. In this case, Δ and τ cannot be determined independently, and the term contributes to a homogeneous Lorentzian line shape with a fwhm width of $\Gamma = \Delta^2\tau = 1/\pi T_2$. There are also contributions to the homogeneous line width from population and orientational relaxation. Here because of the slow population relaxation and the extremely small extent of orientational relaxation, these contributions are negligible. On the other hand, if $\Delta_i \times \tau_i \gg 1$, the term contributes to the inhomogeneous Gaussian line shape with a fwhm of $2.355 \times \Delta_i$. The overall line shape is a convolution of line shapes arising from each term in the summation of eq 4.

The observed CLS is the normalized FFCF; that is, it begins with a maximum possible value of 1 and decays to zero. The time constants obtained from the CLS are the same as the time constants in the FFCF (eq 4). The deviation of the CLS from 1 at T_w = 0 is related to the homogeneous line width, Γ.[46,47] By combining the CLS with the linear absorption spectrum, the full FFCF is obtained including Γ and the Δ_i in units of frequency. In the 2D IR experiments, the observation time is limited by the vibrational lifetime of the μ_2-OD stretching mode. If a decay component, τ_i, is very long compared to the vibrational lifetime, it will appear as a constant offset in the CLS and is represented in the FFCF as a Δ_i^2 with no associated exponential; that is, the exponential time constant is effectively infinite.

As discussed in section D, the spectral diffusion of μ_2-OD bound to guest molecules occurs on three distinguishable time scales: <ps dynamics caused by the local hydrogen bond fluctuation (observed for BzCN, PhSeCN, and benzene), ~ps dynamics associated with the framework structural fluctuation (with benzene, cyclohexane, and the empty pore), and the slower dynamics (≫ps) presumably caused by major reconfiguration of the guest molecules in the pores or slower framework dynamics such as linker rearrangement. In addition, there can be static inhomogeneity caused by framework defects. Based on these observations, the FFCF for the μ_2-OD takes the form

$$\langle \delta\omega(0)\delta\omega(t)\rangle = \frac{\delta(t)}{T_2} + \Delta_{\text{subps}}^2 e^{-t/\tau_{\text{subps}}} + \Delta_{\text{ps}}^2 e^{-t/\tau_{\text{ps}}} + \sum_i \Delta_{\text{slow},i}^2 e^{-t/\tau_{\text{slow},i}} \quad (5)$$

where τ_{subps}, τ_{ps}, and $\tau_{\text{slow},i}$ are observed CLS decay time constants in Figures 7 and 8 (and thus FFCF decay time constants) corresponding to subpicosecond, picosecond, and slower dynamics. Δ_{subps}, Δ_{ps}, and $\Delta_{\text{slow},i}$ are the corresponding spectral diffusion amplitudes for each time scale. Dynamics that satisfy $\Delta_i \times \tau_i < 1$ combine to give the first term, $\delta(t)/T_2$, which gives rise to the homogeneous line width. To determine Δ_{subps}, Δ_{ps}, and $\Delta_{\text{slow},i}$ and T_2, these parameters were varied to reproduce the observed CLS decays in Figure 7 and the 1D line widths in Figure 2B. The detailed procedure to calculate the 1D and 2D spectra based on FFCF has been described in a previous publication.[46,49]

Figure 9 shows the frequency-fluctuation amplitudes of the fast FFCF component (Δ_{subps}) for each guest molecule. As seen in Figure 9, the Δ_{subps} dynamics are very well correlated with the hydrogen bond strength as shown by the spectral peak shift in Figure 2A. The trend in Figure 9 is in agreement with the assignment of the fastest dynamics to hydrogen bond fluctuation; the subpicosecond dynamics can be regarded as a signature of hydrogen bond formation. All of the FFCF parameters are given in Table 1. The other Δs and Γ show little correlation as can be seen in Table 1.

Also seen in Table 1 is the line broadening for μ_2-OD with BzCN as the guest is dominated by Δ_{subps}, the local hydrogen bond fluctuation. When a strong hydrogen bond is formed between a μ_2-OD and a guest molecule, the resonant vibrational frequency becomes very sensitive to the length of

DOI: 10.1021/acs.jpcc.7b02458
J. Phys. Chem. C 2017, 121, 11880−11890

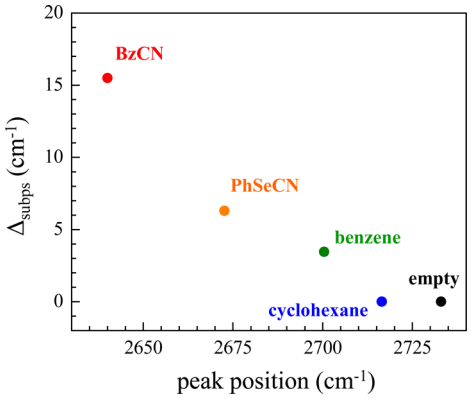

Figure 9. Frequency-fluctuation amplitudes of the fast FFCF component (Δ_{subps}) for each guest molecule. The Δ_{subps} are very well correlated with the hydrogen bond strength.

Table 1. FFCF Frequency Fluctuation Amplitudes

guest	Γ (cm^{-1})	Δ_{subps} (cm^{-1})	Δ_{ps} (cm^{-1})	Δ_{slow} (cm^{-1})
BzCN	0.16	15.5	0	6.4
PhSeCN	4.2	6.3	0	3.1
benzene	0.1	3.5	2.0	6.2
cyclohexane	2.3	0	3.5	2.8
empty	3.8	0	1.7	1.8

*Definition of each parameter follows eq 5. $\Gamma = 1/\pi T_2$ provides purely homogeneous line width in fwhm. Other fluctuation amplitudes broaden the bands inhomogeneously. Δ_{slow} is defined as $\Delta_{slow} = \sqrt{\sum_i \Delta_{slow,i}^2}$. The corresponding time constants can be found in Figure 7 (for slow dynamics) and Figure 8 (for subps and ps dynamics).

the hydrogen bond. Small variations of the length cause a large shift in the resonant frequency, leading to the broad 1D line shape. Thus, the large 1D line width is another indication of hydrogen bond formation between μ_2-OD and a guest molecule.

Δ_{slow} (Table 1) is weakly correlated to the hydrogen bonding strength, except for benzene which shows an exceptionally large Δ_{slow}. The large Δ_{slow} for benzene may result from its relatively small size; various configurations of benzene in the pore may be allowed as it is much smaller than the other hydrogen bonding molecules. A range of configurations could lead to the large inhomogeneity observed in the hydroxyl's absorption band with benzene.

F. Oscillatory Dynamics of the Hydrogen Bond between μ_2-OD and Benzonitrile. As discussed in section D, when BzCN is the guest in the pores, the CLS shows an underdamped oscillation (see Figure 10A) with a period of ~1.5 ps. Fourier transform of the CLS (Figure 10B) yields the oscillation frequency of 17−30 cm^{-1}. Several possible artifacts that can distort 2D band shapes at early time were investigated, including the nonresonant signal or diffraction saturation effects in the pulse shaper AOM. These possible artifacts were ruled out. Spectral diffusion caused by random frequency fluctuations cause the CLS to decay monotonically and will not cause oscillations. Oscillations have been reported in other hydrogen bonding systems.[11,22,27]

Previously for the O−H vibration of HOD in D_2O, it was theoretically suggested and later experimentally verified that the FFCF shows an ~170 cm^{-1} oscillation due to hindered translations of water molecules, which produce an oscillation in

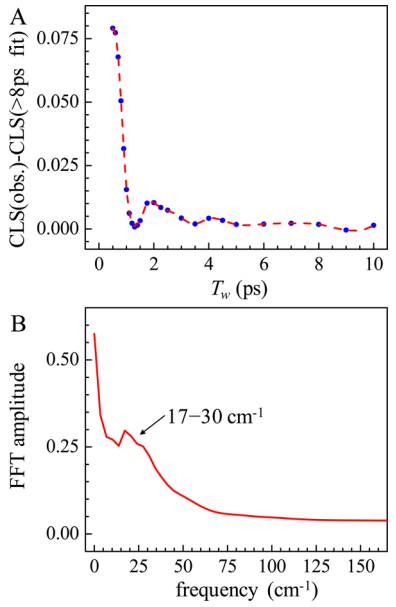

Figure 10. (A) Dots and dotted line: the early time CLS decay for μ_2-OD bound to BzCN showing an oscillation. (B) Fast Fourier transform (FFT) amplitude extracted from the CLS. The broad peak around 17−30 cm^{-1} arises from the oscillatory feature observed in (A).

the hydrogen bond length.[14] In water, the oscillation is in the distance between two water molecules that is quantified by the oxygen−oxygen distance. In the MOF system, the distance between the oxygen in μ_2-OD and the nitrogen in BzCN can oscillate, causing the hydrogen bond length (strength) to oscillate, which in turn causes the frequency to oscillate. The much lower oscillation frequency of ~20 cm^{-1} (compared with ~170 cm^{-1} observed in bulk water) may be caused by the large mass of BzCN and a weaker hydrogen bond compared with the hydrogen bond interaction in bulk water. Another interesting possibility is that the hydrogen bonding interaction between the μ_2-OD and BzCN is coupled to one of the well-defined low-frequency collective vibrational modes (phonons) of the MIL-53(Al) framework; i.e., the lattice vibration is modulating the hydrogen bond strength. Tan and co-workers calculated the low-frequency collective vibrational modes of HKUST-1 MOF and showed that there are vibrational modes as low as ~16 cm^{-1}.[50] The interactions of guest molecules and the μ_2-hydroxyl is believed to induce deformations of the MOF's lattice structure.[5] Then coupling between the guest−framework hydrogen bond and low-frequency phonons could play a significant role in the deformation.

III. CONCLUDING REMARKS

In this paper, we provided clear evidence that guest molecule hydrogen bond acceptors in MIL-53(Al) pores are forming hydrogen bonds with μ_2-ODs in the framework. This system displays hydrogen bond behavior consistent with varying hydrogen bond strengths, and time-averaged and dynamical parameters are well correlated with the hydrogen bond strength. 2D IR spectroscopy revealed the unique dynamical nature of these hydrogen bond interactions. Further studies of these key hydrogen bond interactions could lead to understanding of the fundamental origin of "flexibility" in some MOFs.

DOI: 10.1021/acs.jpcc.7b02458
J. Phys. Chem. C 2017, 121, 11880−11890

It is instructive to compare the 2D IR results on MIL-53(Al) with the dynamics previously observed for UiO-66 MOF functionalized with an iron−carbonyl complex as the vibrational probe.[23] In the functionalized UiO-66 MOF, the spectral diffusion in the carbonyl stretch mode was observed on the time scale of ≥7 ps, demonstrating that some dynamical elasticity exists even in the relatively stiff UiO-66 MOF. The 2D IR measurements on the bridging hydroxyls in the flexible MIL-53(Al) showed distinct results. The spectral diffusions on much faster time scales (<2 ps) were observed, which likely arise from fluctuations of the more flexible framework and/or local hydrogen bond dynamics.

The bridging hydroxyl as vibrational probe permitted the direct observation of the framework−guest hydrogen bond interactions without perturbing the framework structure. Accordingly, the results are directly comparable with molecular dynamics simulations using force fields for the native frameworks, which have recently been studied intensively and developed for a variety of MOFs.[24,25] As hydroxyl groups in frameworks can be found in many other types of MOFs, the experimental scheme developed here will be applicable to elucidate the dynamical natures of a variety of MOFs.

■ ASSOCIATED CONTENT

Supporting Information

The Supporting Information is available free of charge on the ACS Publications website at DOI: 10.1021/acs.jpcc.7b02458.

Figures S1−S6 (PDF)

■ AUTHOR INFORMATION

Corresponding Author

*Phone 650 723-4446; e-mail fayer@stanford.edu (M.D.F.).

ORCID

Jun Nishida: 0000-0001-7834-8179

Michael D. Fayer: 0000-0002-0021-1815

Notes

The authors declare no competing financial interest.

■ ACKNOWLEDGMENTS

This material is based upon work supported by the Air Force Office of Scientific Research under AFOSR Award No. FA9550-16-1-0104. We thank Chang Yan and Rongfeng Yuan for their experimental assistance in the sample preparation and the ultrafast infrared spectroscopy experiments, Steven Yamada for his assistance in FFCF analysis, and Dr. Daiki Umeyama and Patrick Kramer for many useful discussions.

■ REFERENCES

(1) Li, J. R.; Kuppler, R. J.; Zhou, H. C. Selective Gas Adsorption and Separation in Metal−Organic Frameworks. *Chem. Soc. Rev.* **2009**, *38*, 1477−1504.

(2) Van de Voorde, B.; Bueken, B.; Denayer, J.; De Vos, D. Adsorptive Separation on Metal−Organic Frameworks in the Liquid Phase. *Chem. Soc. Rev.* **2014**, *43*, 5766−5788.

(3) Cavka, J. H.; Jakobsen, S.; Olsbye, U.; Guillou, N.; Lamberti, C.; Bordiga, S.; Lillerud, K. P. A New Zirconium Inorganic Building Brick Forming Metal Organic Frameworks with Exceptional Stability. *J. Am. Chem. Soc.* **2008**, *130*, 13850−13851.

(4) Pullen, S.; Fei, H.; Orthaber, A.; Cohen, S. M.; Ott, S. Enhanced Photochemical Hydrogen Production by a Molecular Diiron Catalyst Incorporated into a Metal−Organic Framework. *J. Am. Chem. Soc.* **2013**, *135*, 16997−17003.

(5) Serre, C.; Millange, F.; Thouvenot, C.; Noguès, M.; Marsolier, G.; Louër, D.; Férey, G. Very Large Breathing Effect in the First Nanoporous Chromium (III)-based Solids: MIL-53 or $Cr^{III}(OH)\cdot\{O_2C\text{-}C_6H_4\text{-}CO_2\}\cdot\{HO_2C\text{-}C_6H_4\text{-}CO_2H\}_x\cdot H_2O_y$. *J. Am. Chem. Soc.* **2002**, *124*, 13519−13526.

(6) Férey, G.; Serre, C. Large Breathing Effects in Three-Dimensional Porous Hybrid Matter: Facts, Analyses, Rules and Consequences. *Chem. Soc. Rev.* **2009**, *38*, 1380−1399.

(7) Horike, S.; Shimomura, S.; Kitagawa, S. Soft Porous Crystals. *Nat. Chem.* **2009**, *1*, 695−704.

(8) Loiseau, T.; Serre, C.; Huguenard, C.; Fink, G.; Taulelle, F.; Henry, M.; Bataille, T.; Férey, G. A Rationale for the Large Breathing of the Porous Aluminum Terephthalate (MIL-53) Upon Hydration. *Chem. - Eur. J.* **2004**, *10*, 1373−1382.

(9) Bourrelly, S.; Moulin, B.; Rivera, A.; Maurin, G.; Devautour-Vinot, S.; Serre, C.; Devic, T.; Horcajada, P.; Vimont, A.; Clet, G.; et al. Explanation of the Adsorption of Polar Vapors in the Highly Flexible Metal Organic Framework MIL-53 (Cr). *J. Am. Chem. Soc.* **2010**, *132*, 9488−9498.

(10) Arunan, E.; Desiraju, G. R.; Klein, R. A.; Sadlej, J.; Scheiner, S.; Alkorta, I.; Clary, D. C.; Crabtree, R. H.; Dannenberg, J. J.; Hobza, P.; et al. Definition of the Hydrogen Bond (IUPAC Recommendations 2011). *Pure Appl. Chem.* **2011**, *83*, 1637−1641.

(11) Asbury, J. B.; Steinel, T.; Stromberg, C.; Corcelli, S. A.; Lawrence, C. P.; Skinner, J. L.; Fayer, M. D. Water Dynamics: Vibrational Echo Correlation Spectroscopy and Comparison to Molecular Dynamics Simulations. *J. Phys. Chem. A* **2004**, *108*, 1107−1119.

(12) Woutersen, S.; Bakker, H. J. Resonant Intermolecular Transfer of Vibrational Energy in Liquid Water. *Nature* **1999**, *402*, 507−509.

(13) Woutersen, S.; Emmerichs, U.; Bakker, H. J. Femtosecond Mid-IR Pump-probe Spectroscopy of Liquid Water: Evidence for a Two-Component Structure. *Science* **1997**, *278*, 658−660.

(14) Fecko, C.; Eaves, J.; Loparo, J.; Tokmakoff, A.; Geissler, P. Ultrafast Hydrogen-Bond Dynamics in the Infrared Spectroscopy of Water. *Science* **2003**, *301*, 1698−1702.

(15) Woutersen, S.; Mu, Y.; Stock, G.; Hamm, P. Subpicosecond Conformational Dynamics of Small Peptides Probed by Two-Dimensional Vibrational Spectroscopy. *Proc. Natl. Acad. Sci. U. S. A.* **2001**, *98*, 11254−11258.

(16) Mukherjee, P.; Kass, I.; Arkin, I. T.; Zanni, M. T. Picosecond Dynamics of a Membrane Protein Revealed by 2D IR. *Proc. Natl. Acad. Sci. U. S. A.* **2006**, *103*, 3528−3533.

(17) King, J. T.; Kubarych, K. J. Site-Specific Coupling of Hydration Water and Protein Flexibility Studied in Solution with Ultrafast 2D-IR Spectroscopy. *J. Am. Chem. Soc.* **2012**, *134*, 18705−18712.

(18) Ma, J.; Pazos, I. M.; Gai, F. Microscopic Insights into the Protein-Stabilizing Effect of Trimethylamine N-oxide (TMAO). *Proc. Natl. Acad. Sci. U. S. A.* **2014**, *111*, 8476−8481.

(19) Stevenson, P.; Tokmakoff, A. Ultrafast Fluctuations of High Amplitude Electric Fields in Lipid Membranes. *J. Am. Chem. Soc.* **2017**, *139*, 4743−4752.

(20) King, J. T.; Ross, M. R.; Kubarych, K. J. Ultrafast α-Like Relaxation of a Fragile Glass-forming Liquid Measured Using Two-Dimensional Infrared Spectroscopy. *Phys. Rev. Lett.* **2012**, *108*, 157401.

(21) Ren, Z.; Brinzer, T.; Dutta, S.; Garrett-Roe, S. Thiocyanate as a Local Probe of Ultrafast Structure and Dynamics in Imidazolium-Based Ionic Liquids: Water-Induced Heterogeneity and Cation-Induced Ion Pairing. *J. Phys. Chem. B* **2015**, *119*, 4699−4712.

(22) Kramer, P. L.; Giammanco, C. H.; Fayer, M. D. Dynamics of Water, Methanol, and Ethanol in a Room Temperature Ionic Liquid. *J. Chem. Phys.* **2015**, *142*, 212408.

(23) Nishida, J.; Tamimi, A.; Fei, H.; Pullen, S.; Ott, S.; Cohen, S. M.; Fayer, M. D. Structural Dynamics inside a Functionalized Metal−Organic Framework Probed by Ultrafast 2D IR Spectroscopy. *Proc. Natl. Acad. Sci. U. S. A.* **2014**, *111*, 18442−18447.

(24) Medders, G. R.; Paesani, F. Water Dynamics in Metal-Organic Frameworks: Effects of Heterogeneous Confinement Predicted by Computational Spectroscopy. *J. Phys. Chem. Lett.* **2014**, *5*, 2897−2902.

(25) Grosch, J. S.; Paesani, F. Molecular-Level Characterization of the Breathing Behavior of the Jungle-Gym-type DMOF-1 Metal−Organic Framework. *J. Am. Chem. Soc.* **2012**, *134*, 4207−4215.
(26) Salazar, J.; Weber, G.; Simon, J.; Bezverkhyy, I.; Bellat, J. Characterization of Adsorbed Water in MIL-53 (Al) by FTIR Spectroscopy and Ab-initio Calculations. *J. Chem. Phys.* **2015**, *142*, 124702.
(27) Yan, C.; Nishida, J.; Yuan, R.; Fayer, M. D. Water of Hydration Dynamics in Minerals Gypsum and Bassanite: Ultrafast 2D IR Spectroscopy of Rocks. *J. Am. Chem. Soc.* **2016**, *138*, 9694−9703.
(28) Shim, S.-H.; Zanni, M. T. How to Turn Your Pump-Probe Instrument into a Multidimensional Spectrometer: 2D IR and Vis Spectroscopies Via Pulse Shaping. *Phys. Chem. Chem. Phys.* **2009**, *11*, 748−761.
(29) Kumar, S. K. K.; Tamimi, A.; Fayer, M. D. Comparisons of 2D IR Measured Spectral Diffusion in Rotating Frames Using Pulse Shaping and in the Stationary Frame Using the Standard Method. *J. Chem. Phys.* **2012**, *137*, 184201.
(30) Falk, M.; Whalley, E. Infrared Spectra of Methanol and Deuterated Methanols in Gas, Liquid, and Solid Phases. *J. Chem. Phys.* **1961**, *34*, 1554−1568.
(31) Zheng, J. R.; Kwak, K.; Asbury, J.; Chen, X.; Piletic, I. R.; Fayer, M. D. Ultrafast Dynamics of Solute-solvent Complexation Observed at Thermal Equilibrium in Real Time. *Science* **2005**, *309*, 1338−1343.
(32) Saggu, M.; Levinson, N. M.; Boxer, S. G. Direct Measurements of Electric Fields in Weak OH··· π Hydrogen Bonds. *J. Am. Chem. Soc.* **2011**, *133*, 17414−17419.
(33) Fried, S. D.; Boxer, S. G. Measuring Electric Fields and Noncovalent Interactions Using the Vibrational Stark Effect. *Acc. Chem. Res.* **2015**, *48*, 998−1006.
(34) Kubo, R. A Stochastic Theory of Line Shapes. *Adv. Chem. Phys.* **1969**, *15*, 101−127.
(35) Schmidt, J.; Corcelli, S.; Skinner, J. Pronounced Non-Condon Effects in the Ultrafast Infrared Spectroscopy of Water. *J. Chem. Phys.* **2005**, *123*, 044513.
(36) Tokmakoff, A. Orientational Correlation Functions and Polarization Selectivity for Nonlinear Spectroscopy of Isotropic Media. I. Third Order. *J. Chem. Phys.* **1996**, *105*, 1−12.
(37) Lipari, G.; Szabo, A. Effect of Librational Motion on Fluorescence Depolarization and Nuclear Magnetic-Resonance Relaxation in Macromolecules and Membranes. *Biophys. J.* **1980**, *30*, 489−506.
(38) Wang, C. C.; Pecora, R. Time-Correlation Functions for Restricted Rotational Diffusion. *J. Chem. Phys.* **1980**, *72*, 5333−5340.
(39) Rezus, Y. L. A.; Bakker, H. J. On the Orientational Relaxation of HDO in Liquid Water. *J. Chem. Phys.* **2005**, *123*, 114502.
(40) Steinel, T.; Asbury, J. B.; Zheng, J.; Fayer, M. D. Watching Hydrogen Bonds Break: A Transient Absorption Study of Water. *J. Phys. Chem. A* **2004**, *108*, 10957−10964.
(41) Kenkre, V. M.; Tokmakoff, A.; Fayer, M. D. Theory of Vibrational-Relaxation of Polyatomic-Molecules in Liquids. *J. Chem. Phys.* **1994**, *101*, 10618−10629.
(42) Kinosita, K., Jr.; Kawato, S.; Ikegami, A. A Theory of Fluorescence Polarization Decay in Membranes. *Biophys. J.* **1977**, *20*, 289−305.
(43) Tan, H.-S.; Piletic, I. R.; Fayer, M. Orientational Dynamics of Water Confined on a Nanometer Length Scale in Reverse Micelles. *J. Chem. Phys.* **2005**, *122*, 174501.
(44) Hamm, P.; Zanni, M. T. *Concepts and Methods of 2D Infrared Spectroscopy*; Cambridge University Press: New York, 2011.
(45) Baiz, C. R.; Schach, D.; Tokmakoff, A. Ultrafast 2D IR Microscopy. *Opt. Express* **2014**, *22*, 18724−18735.
(46) Kwak, K.; Park, S.; Finkelstein, I. J.; Fayer, M. D. Frequency-Frequency Correlation Functions and Apodization in Two-Dimensional Infrared Vibrational Echo Spectroscopy: A New Approach. *J. Chem. Phys.* **2007**, *127*, 124503.
(47) Kwak, K.; Rosenfeld, D. E.; Fayer, M. D. Taking Apart the Two-Dimensional Infrared Vibrational Echo Spectra: More Information and Elimination of Distortions. *J. Chem. Phys.* **2008**, *128*, 204505.
(48) Kolokolov, D. I.; Jobic, H.; Stepanov, A. G.; Guillerm, V.; Devic, T.; Serre, C.; Férey, G. Dynamics of Benzene Rings in MIL-53 (Cr) and MIL-47 (V) Frameworks Studied by ^{2}H NMR Spectroscopy. *Angew. Chem., Int. Ed.* **2010**, *49*, 4791−4794.
(49) Mukamel, S. *Principles of Nonlinear Optical Spectroscopy*; Oxford University Press: New York, 1995.
(50) Ryder, M. R.; Civalleri, B.; Cinque, G.; Tan, J.-C. Discovering Connections between Terahertz Vibrations and Elasticity Underpinning the Collective Dynamics of the HKUST-1 Metal−Organic Framework. *CrystEngComm* **2016**, *18*, 4303−4312.

DOI: 10.1021/acs.jpcc.7b02458
J. Phys. Chem. C 2017, 121, 11880−11890